Three-dimensional multi-photon direct laser writing with variable repetition rate

Joachim Fischer,[1,*] Jonathan B. Mueller,[2] Johannes Kaschke,[2] Thomas J. A. Wolf,[3,4] Andreas-Neil Unterreiner,[3,4] and Martin Wegener[1,2,4]

[1] *Institut für Nanotechnologie, Karlsruhe Institute of Technology (KIT), D-76021 Karlsruhe, Germany*
[2] *Institut für Angewandte Physik, KIT, Wolfgang-Gaede-Str. 1, D-76131 Karlsruhe, Germany*
[3] *Institut für Physikalische Chemie, KIT, D-76128 Karlsruhe, Germany*
[4] *DFG-Center for Functional Nanostructures (CFN), KIT, D-76128 Karlsruhe, Germany*
[*] *joachim.fischer@kit.edu*

Abstract: We perform multi-photon direct laser writing as a function of laser repetition rate over many orders of magnitude and otherwise unchanged experimental conditions. These new data serve as basis for investigating the influence of different proposed mechanisms involved in the photopolymerization: two-photon absorption, photoionization, avalanche ionization and heat accumulation. We find different non-linearities for high and low repetition rates consistent with different initiation processes being involved. The scaling of the resulting linewidths, however, is neither expected nor found to depend on repetition rate or non-linearity.

OCIS codes: (350.3390) Laser materials processing; (350.3450) Laser-induced chemistry; (050.5298) Photonic crystals.

References and links

1. H. B. Sun, S. Matsuo, and H. Misawa, "Three-dimensional photonic crystal structures achieved with two-photon-absorption photopolymerization of resin," Appl. Phys. Lett. **74**, 786–788 (1999).
2. S. Kawata, H. B. Sun, T. Tanaka, and K. Takada, "Finer features for functional microdevices," Nature **412**, 697–698 (2001).
3. M. Straub and M. Gu, "Near-infrared photonic crystals with higher-order bandgaps generated by two-photon photopolymerization," Opt. Lett. **27**, 1824–1826 (2002).
4. M. Deubel, G. von Freymann, M. Wegener, S. Pereira, K. Busch, and C. M. Soukoulis, "Direct laser writing of three-dimensional photonic-crystal templates for telecommunications," Nature Mater. **3**, 444–447 (2004).
5. K. K. Seet, S. Juodkazis, V. Jarutis, and H. Misawa, "Feature-size reduction of photopolymerized structures by femtosecond optical curing of SU-8," Appl. Phys. Lett. **89**, 024106–024106 (2006).
6. J.-F. Xing, X.-Z. Dong, W.-Q. Chen, X.-M. Duan, N. Takeyasu, T. Tanaka, and S. Kawata, "Improving spatial resolution of two-photon microfabrication by using photoinitiator with high initiating efficiency," Appl. Phys. Lett. **90**, 131106–131106 (2007).
7. S. H. Park, T. W. Lim, D.-Y. Yang, R. H. Kim, and K.-S. Lee, "Improvement of spatial resolution in nano-stereolithography using radical quencher," Macromol. Res. **14**, 559–564 (2006).
8. M. Malinauskas, A. Žukauskas, G. Bičkauskaitė, R. Gadonas, and S. Juodkazis, "Mechanisms of three-dimensional structuring of photo-polymers by tightly focussed femtosecond laser pulses," Opt. Express **18**, 10209–10221 (2010).
9. M. Malinauskas, P. Danilevičius, and S. Juodkazis, "Three-dimensional micro-/nano-structuring via direct write polymerization with picosecond laser pulses," Opt. Express **19**, 5602–5610 (2011).
10. J. Fischer and M. Wegener, "Three-dimensional direct laser writing inspired by stimulated-emission-depletion microscopy," Opt. Mater. Express **1**, 614–624 (2011).

#195297 - $15.00 USD Received 6 Aug 2013; revised 14 Oct 2013; accepted 15 Oct 2013; published 25 Oct 2013

11. J. Fischer and M. Wegener, "Three-dimensional optical laser lithography beyond the diffraction limit," Laser Photon. Rev. **7**, 22–44 (2013).
12. S. W. Hell and J. Wichmann, "Breaking the diffraction resolution limit by stimulated emission: Stimulated-emission-depletion fluorescence microscopy," Opt. Lett. **19**, 780–782 (1994).
13. H.-B. Sun and S. Kawata, "Two-photon laser precision microfabrication and its applications to micro-nano devices and systems," J. Lightwave Technol. **21**, 624 (2003).
14. T. Baldacchini, S. Snider, and R. Zadoyan, "Two-photon polymerization with variable repetition rate bursts of femtosecond laser pulses," Opt. Express **20**, 29890–29899 (2012).
15. J. B. Mueller, J. Fischer, Y. J. Mange, T. Nann, and M. Wegener, "In-situ local temperature measurement during three-dimensional direct laser writing," Appl. Phys. Lett. **103**, 123107 (2013).
16. S. Eaton, H. Zhang, P. Herman, F. Yoshino, L. Shah, J. Bovatsek, and A. Arai, "Heat accumulation effects in femtosecond laser-written waveguides with variable repetition rate," Opt. Express **13**, 4708–4716 (2005).
17. M. Emons, K. Obata, T. Binhammer, A. Ovsianikov, B. N. Chichkov, and U. Morgner, "Two-photon polymerization technique with sub-50 nm resolution by sub-10 fs laser pulses," Opt. Mater. Express **2**, 942–947 (2012).
18. M. Malinauskas, M. Farsari, A. Piskarskas, and S. Juodkazis, "Ultrafast laser nanostructuring of photopolymers: A decade of advances," Phys. Rep., doi: 10.1016/j.physrep.2013.07.005 (2013).
19. M. Thiel, J. Fischer, G. von Freymann, and M. Wegener, "Direct laser writing of three-dimensional submicron structures using a continuous-wave laser at 532 nm," Appl. Phys. Lett. **97**, 221102 (2010).
20. C. Decker and K. Moussa, "Real-time kinetic study of laser-induced polymerization," Macromolecules **22**, 4455–4462 (1989).
21. J. Fischer, G. von Freymann, and M. Wegener, "The materials challenge in diffraction-unlimited direct-laser-writing optical lithography," Adv. Mater. **22**, 3578–3582 (2010).
22. M. J. Frisch, G. W. Trucks, H. B. Schlegel, G. E. Scuseria, M. A. Robb, J. R. Cheeseman, G. Scalmani, V. Barone, B. Mennucci, G. A. Petersson, H. Nakatsuji, M. Caricato, X. Li, H. P. Hratchian, A. F. Izmaylov, J. Bloino, G. Zheng, J. L. Sonnenberg, M. Hada, M. Ehara, K. Toyota, R. Fukuda, J. Hasegawa, M. Ishida, T. Nakajima, Y. Honda, O. Kitao, H. Nakai, T. Vreven, J. A. Montgomery, Jr., J. E. Peralta, F. Ogliaro, M. Bearpark, J. J. Heyd, E. Brothers, K. N. Kudin, V. N. Staroverov, R. Kobayashi, J. Normand, K. Raghavachari, A. Rendell, J. C. Burant, S. S. Iyengar, J. Tomasi, M. Cossi, N. Rega, J. M. Millam, M. Klene, J. E. Knox, J. B. Cross, V. Bakken, C. Adamo, J. Jaramillo, R. Gomperts, R. E. Stratmann, O. Yazyev, A. J. Austin, R. Cammi, C. Pomelli, J. W. Ochterski, R. L. Martin, K. Morokuma, V. G. Zakrzewski, G. A. Voth, P. Salvador, J. J. Dannenberg, S. Dapprich, A. D. Daniels, . Farkas, J. B. Foresman, J. V. Ortiz, J. Cioslowski, and D. J. Fox, "Gaussian 09 Revision A.2," Gaussian Inc. Wallingford CT 2009.
23. F. Weigend, F. Furche, and R. Ahlrichs, "Gaussian basis sets of quadruple zeta valence quality for atoms H–Kr," J. Chem. Phys. **119**, 12753 (2003).
24. O. F. Olaj, I. Bitai, and F. Hinkelmann, "The laser-flash-initiated polymerization as a tool of evaluating (individual) kinetic constants of free-radical polymerization, 2. the direct determination of the rate of constant of chain propagation," Macromol. Chem. Phys. **188**, 1689–1702 (1987).
25. J. Fischer and M. Wegener, "Ultrafast polymerization inhibition by stimulated emission depletion for three-dimensional nano lithography," Adv. Materials **24**, OP65–OP69 (2012).
26. K. J. Schafer, J. M. Hales, M. Balu, K. D. Belfield, E. W. Van Stryland, and D. J. Hagan, "Two-photon absorption cross-sections of common photoinitiators," J. Photochem. Photobiol. A **162**, 497–502 (2004).
27. M. Pawlicki, H. A. Collins, R. G. Denning, and H. L. Anderson, "Two-photon absorption and the design of two-photon dyes," Angew. Chem. Int. Ed. **48**, 3244–3266 (2009).
28. S. Juodkazis, V. Mizeikis, K. K. Seet, M. Miwa, and H. Misawa, "Two-photon lithography of nanorods in SU-8 photoresist," Nanotechnology **16**, 846 (2005).
29. D. Tan, Y. Li, F. Qi, H. Yang, Q. Gong, X. Dong, and X. Duan, "Reduction in feature size of two-photon polymerization using SCR500," Appl. Phys. Lett. **90**, 071106–071106 (2007).
30. A. Pikulin and N. Bityurin, "Spatial confinement of percolation: Monte Carlo modeling and nanoscale laser polymerization," Phys. Rev. B **82**, 085406 (2010).

1. Introduction

Three-dimensional direct laser writing (3D DLW) is a versatile lithography approach that allows for the fabrication of a large variety of complex polymeric micro- and nanostructures [1, 2, 3, 4]. From the very beginning [2], DLW has been used to produce sub-wavelength feature sizes. During the last decade, the impact of several experimental parameters has been examined in order to increase the photoresists' resolution [5, 6, 7, 8, 9]. While improved feature sizes have been demonstrated using a photoresist with higher sensitivity [6] other results have indicated that completely unsensitized photoresists offer the smallest features [8]. Moreover, it has been observed that high repetition rates and short pulses lead to higher structure quality [9].

#195297 - $15.00 USD Received 6 Aug 2013; revised 14 Oct 2013; accepted 15 Oct 2013; published 25 Oct 2013

Despite all these improvements, the diffraction limit has been broken only recently [10, 11] using an special DLW approach inspired by super-resolution microscopy [12].

The classical picture of the DLW process is based on multi-photon absorption of photoinitiator molecules and subsequent chemical bond breaking [13]. For example, radical-based negative-tone photoresists for DLW consist of a polymerizable substance (*e.g.*, monomers) and a photoinitiator. The latter efficiently absorbs the laser light *via* multi-photon absorption. After light absorption, the molecules generate initiating radicals with a certain quantum yield. While DLW can be easily understood in a qualitative fashion, a more detailed quantitative understanding of the mechanisms involved is still missing, making further optimization rather difficult. In the simplest model, a volume element of the photoresist withstands the wet-chemical development step in case the local exposure dose $D(\vec{r})$ exceeds a certain threshold value D_{th} (compare [11]). A convenient measure of the exposure dose is the number of photons absorbed per volume, hence, the deposited energy density. This model neglects the complex chemistry of the polymerization reaction as well as the quantum yield of radical/acid generation. Moreover, this local model neglects diffusion of molecules and heat transport.

Recently, it has been proposed that the actual mechanism leading to the generation of initiating radicals is not multi-photon excitation of photoinitiator molecules but multi-photon ionization and subsequent avalanche ionization [8]. Furthermore, a significant [14] or even dominant influence [9] of heat accumulation on the polymerization process in DLW has been proposed. In contrast, very recent *in-situ* temperature measurements have not revealed a significant heating [15]. Notably, such mechanisms are well established in related areas of laser materials-processing [16], yet their influence on DLW has not been unambiguously shown so far. As a consequence, the polymerization behavior for low repetition rates R (*e.g.*, $R = 1\,\mathrm{kHz}$) and high repetition rates (*e.g.*, $R = 80\,\mathrm{MHz}$) should be fundamentally different: In the former case, the temperature rise induced by the absorption of a single laser pulse would fade away before a second laser pulse arrives, whereas in the latter case the temperature could accumulate over many consecutive laser pulses. Along these lines, the authors of reference [9] find a different scaling of the resulting polymer linewidth for $R = 200\,\mathrm{kHz}$ and $R = 500\,\mathrm{kHz}$ which they interpret as a sign for heat-accumulation dominated polymerization at high repetition rates. One should note, however, that they have used picosecond pulses instead of more common femtosecond pulses which hinders a direct comparison with the present paper.

Along these lines, it seems to be common practice [5, 17, 18] to measure the resulting polymer linewidth as a function of the incident laser power while all other processing parameters were kept constant. This data is often used to substantiate statements about the absorption/initiation mechanism. We will show in Section 4, however, that within the above simple threshold model this kind of data does not give any information about the underlying mechanism. Therefore, parameters other than the laser power have to be varied. For example, a variation in writing speed is easy to accomplish [19]. However, as the exposure time (typically between 0.1 ms and 10 ms) and the duration of the local polymerization reaction ($\approx 0.1\,\mathrm{s}$, [20]) are similar, a change in writing speed is hard to interpret as it may be accompanied by changes in the complex non-equilibrium polymerization chemistry. Another very elegant possibility is to use pulse bursts of different burst-repetition rates while keeping the number and energy of the pulses constant [14]. Yet another easy-to-interpret method is to change the laser repetition frequency: For all relevant repetition rates R, the pulse separation ($< 1\,\mathrm{ms}$) is shorter than the duration of the polymerization reaction. In this way, the polymerization dynamics should not be significantly influenced by the repetition rate, as long as the average radical generation rate is kept constant. So far, only few studies on DLW involving different repetition rates have been published [9, 17]. However, a consistent overall picture of the repetition-rate influence is still missing.

#195297 - $15.00 USD Received 6 Aug 2013; revised 14 Oct 2013; accepted 15 Oct 2013; published 25 Oct 2013

In this empirical study, we therefore vary the laser repetition R rate of our DLW system (Section 2) from $R = 80\,\mathrm{MHz}$ down to $R = 1\,\mathrm{kHz}$ and determine the polymerization-threshold and the damage-threshold pulse-energies (Section 3). With a single experimental setup, we cover almost five orders of magnitude in repetition rate and generate a very detailed data set. In particular, the presented data covers the repetition rates of the most commonly used DLW laser sources, namely Ti:Sa oscillators (typically $R = 80\,\mathrm{MHz}$) and Ti:Sa amplifiers (typically $R = 1\,\mathrm{kHz}$). Moreover, we examine the linewidth scaling (Section 4) and the 3D resolution at different repetition rates (Section 5).

2. Experimental

In the following, we investigate four different photoresist compositions A–D. All photoresists are homemade and based on the monomer pentaerythritol triacrylate (PETA, Sigma Aldrich, technical grade). For photoresists B–D, different photoinitiators have been added (see Table 1) while photoresist A is the monomer as received from the supplier. The photoinitiator concentrations have been chosen such that comparable pulse energies can be used for all photoresists. Photoresists B and C contain Irgacure 369 and Irgacure 819, respectively. Photoresist D contains 7-diethylamino-3-thenoylcoumarin (DETC).

Table 1. Photoresists under investigation.

photoresist	monomer	photoinitiator	photoinitiator concentration (% wt)
A	PETA	-	-
B	PETA	Irgacure 369	2
C	PETA	Irgacure 819	2
D	PETA	DETC	0.25

We use a home-built 3D DLW setup (see Fig. 1) based on a Ti:sapphire oscillator (Coherent Chameleon Ultra II) delivering 150 fs pulses centered around 800 nm wavelength. The pulse chirp caused by the optical setup is not compensated and, hence, the pulse duration at the sample position is slightly longer. Using a pulse picker (PulseSelect, APE Berlin), we vary the repetition rate. The pulse energy is controlled by means of an acousto-optic modulator (AOM, AA Optic-Electronic MTS40-A3-750.850). The laser beam is focused through an oil immersion lens with numerical aperture NA = 1.4 (Leica HCX PL APO 100x/1.4-0.7 OIL CS). All pulse energies are measured at the position of the objective lens through an aperture of 5.6 mm diameter, corresponding to the objective lens entrance pupil. The energy values are not corrected for the objective transmittance, which is around 70% according to the data sheet. The focal intensity distribution is measured by scanning a single 100 nm gold bead through the focus and collecting the backscattered light [21]. The objective lens is translated along the optical axis (z-direction) using a piezo stage (Physik Instrumente P-733.ZCL). The sample is translated laterally (x, y-directions) using another piezo stage (Physik Instrumente P-734.2CD).

The photoresists are drop-casted onto a glass cover-slip. During the writing procedure, an additional dedicated diode laser (675 nm wavelength) is used to find the z-position of the glass-photoresist interface with high accuracy *via* a confocal detection scheme. A potential tilt of the surface with respect to the translation stage's movement plane is determined and compensated for. Typical values are below 0.1°. This compensation ensures that all written test lines have a very reproducible z-position with respect to the interface.

All exposures are performed with a scan velocity of $100\,\mu\mathrm{m/s}$. A camera and a transmitted-light illumination with a red light emitting diode are used to observe the exposure process

#195297 - $15.00 USD Received 6 Aug 2013; revised 14 Oct 2013; accepted 15 Oct 2013; published 25 Oct 2013

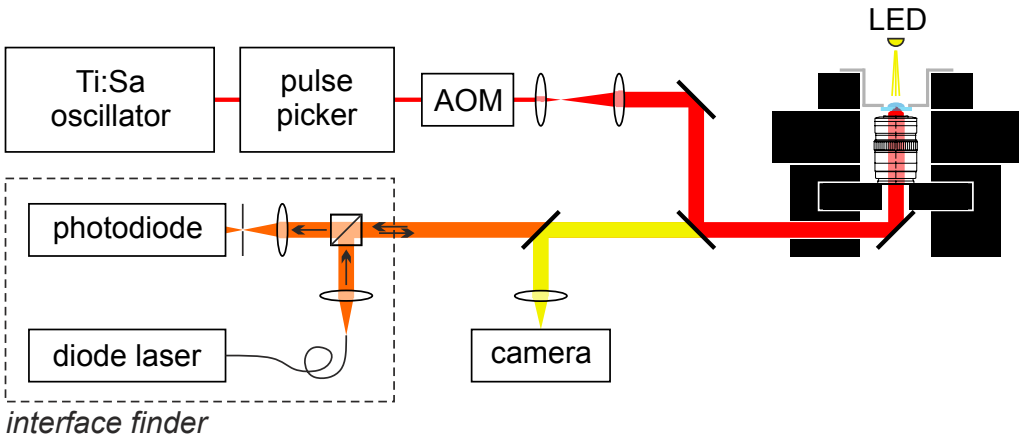

Fig. 1. Scheme of the DLW setup.

in situ. After writing is completed, the samples are developed for 10 minutes in 2-propanol, subsequently rinsed in acetone and water, and blown dry with nitrogen gas.

3. Polymerization and damage threshold

3.1. Polymerization threshold

For the above photoresist compositions, we determine the polymerization-threshold pulse-energy and the damage-threshold pulse-energy for 16 different repetition rates ranging from 1 kHz to 80 MHz. We write a test line pattern at the glass-photoresist interface for every repetition rate. The pattern consists of lines with increasing pulse energies (from under-exposed, through normal exposure, up to the damage threshold) and different z-positions (from focusing into the glass volume to writing within the resist volume without contact to the surface).

The polymerization threshold is defined as the lowest pulse energy that yields well defined polymer lines after the development process. We use dark-field optical microscopy to examine the developed samples and to determine the polymerization threshold. In contrast, the damage threshold is observed on the above video camera during the writing process and judged by the visible occurrence of micro-explosions that appear as opaque bubbles.

The resulting polymerization-threshold energies are depicted in Fig. 2 as red points. As expected, the pulse energies needed for polymerization decrease with increasing repetition rate. This is easily understood since at higher repetition rates, more pulses contribute to the exposure of a single volume element (voxel) and the exposure dose accumulates over many pulses. Therefore, the needed exposure per pulse is lower. Within the above simple threshold model we can predict the scaling of the polymerization-threshold pulse energy: The accumulated exposure dose D_{acc} of a single voxel induced by an N-photon-absorption process is given by

$$D_{\mathrm{acc}} = N_{\mathrm{p}} D_{\mathrm{p}} \propto R E_{\mathrm{p}}^{N}, \tag{1}$$

where N_{p} is the number of incident laser pulses, D_{p} is the exposure dose of a single laser pulse, R is the repetition rate, and E_{p} is the pulse energy. Accordingly, the threshold pulse-energy (E_{th}) needed to reach the threshold dose ($D_{\mathrm{acc}} = D_{\mathrm{th}}$) is given by

$$E_{\mathrm{th}} \propto (D_{\mathrm{th}}/R)^{1/N}. \tag{2}$$

#195297 - $15.00 USD Received 6 Aug 2013; revised 14 Oct 2013; accepted 15 Oct 2013; published 25 Oct 2013

A fit according to this formula would correspond to a straight line in the double-log plots in Fig. 2. The higher the order of the non-linearity, the flatter is the slope of the line. Some examples are drawn as guides to the eye (dashed lines in Fig. 2). As we will see below, however, in some cases the experimental data can not be fitted with this expression using a single N.

It has been suggested that multi-photon photoionization and possibly subsequent avalanche ionization could be the dominating absorption/initiation mechanism in 3D DLW [8, 9]. The authors of these publications state that, in case of dominating avalanche ionization, the absorption mechanism would follow a linear dependence $N = 1$. Within their modeling, the authors take the S_0-S_1 transition energy as ionization potential and assume – in analogy to well-established semiconductor physics – that the resulting excited state exhibits "free carriers" and can lead to avalanche-ionization. However, as the electrons promoted to the S_1 state of a molecule are usually still bound to that molecule, this analogy appears questionable to us. The ionization potential of the molecule should be used instead of the S_0-S_1 transition energy. This quantity is the binding energy of the weakest-bound electron of the molecule. In order to determine the corresponding energies, we have conducted numerical calculations using the outer-valence Green's function (OVGF) method as implemented in Gaussian 09 [22] in combination with a QZVP basis [23] for all molecules contained in the examined photoresists. The resulting energies for the lowest electronic transition as well as for photoionization are listed in Table 2. For convenience we calculate the number of 800 nm photons delivering the same energy. This is the number of photons needed to drive these transitions in a multi-photon absorption process.

It should be noted that not only a simultaneous N-photon absorption process can lead to photoionization. Instead, a multi-photon absorption process from S_0 to S_1 together with consecutive one-photon absorption processes might take place within the duration of a single laser pulse. If the cross-sections for the excited-state absorptions are reasonably high, some of these transitions may saturate and the transition probability will be close to unity, independent of the pulse energy. In such cases, the combined non-linearity N of the photoionization process would be smaller than the number of photons needed for photoionization (see Table 2). However, it must be larger or equal to the number of photons needed for the initial electronic excitation.

Below, we will fit the experimental data under the assumption of several absorption channels contributing to the exposure dose:

$$D_{\mathrm{acc}} = N_{\mathrm{p}} D_{\mathrm{p}} = R \sum a_N {E_{\mathrm{p}}}^N , \tag{3}$$

where the fit coefficients a_N contain the N-photon absorption coefficient, as well as the radical-generation efficiency and the reactivity of the generated radicals. (Precisely, instead of fitting a function $E_{\mathrm{th}}(R)$, we fit a function $R(E_{\mathrm{th}})$ based on the above equation *via* a least-square fit.) For every photoresist, we use two absorption channels with N-values taken from Table 2 corresponding to multi-photon excitation and multi-photon photoionization of the molecules.

An alternative description of the absorption process as a tunnel ionization appears unreasonable: The corresponding Keldysh parameter γ for the highest threshold pulse-energy (3.2 nJ, see Fig. 2) and the lowest ionization potential (7.9 eV, see Table 2) is $\gamma = 2.77$. A tunnel-ionization is expected only for $\gamma \ll 1$, corresponding to $E_{\mathrm{p}} \gg 25$ nJ (assuming 200 fs pulse duration at the sample and a diffraction-limited laser spot).

3.1.1. Photoresist A

When writing into the pure monomer (photoresist A), only low repetition rates ≤ 128 kHz lead to well-defined structures. When using high repetition rates, we only observe uncontrolled micro-explosions. In this photoresist, only the monomer molecules can absorb the laser light. We fit the repetition-rate dependence using the relation $D_{\mathrm{acc}} = a_3 \cdot {E_{\mathrm{p}}}^3 + a_7 \cdot {E_{\mathrm{p}}}^7$, corresponding to a three-photon absorption for an S_0-S_1 excitation and a seven-photon absorption for

#195297 - $15.00 USD Received 6 Aug 2013; revised 14 Oct 2013; accepted 15 Oct 2013; published 25 Oct 2013

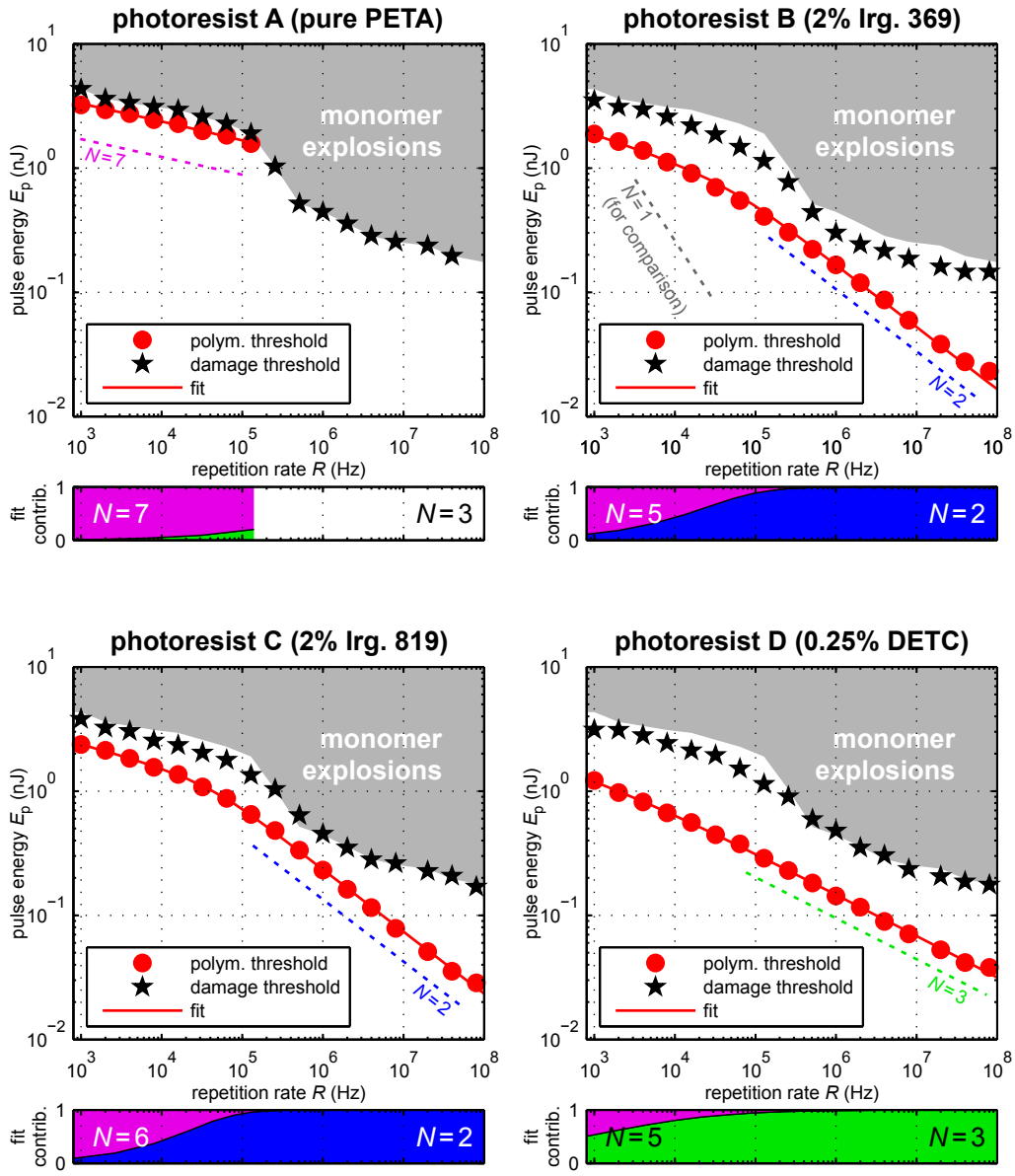

Fig. 2. Polymerization and damage thresholds of the different photoresists for different repetition rates (at 100 µm/s scan velocity). The damage threshold of the pure monomer is plotted as gray area in all panels. The solid red lines are fits to the experimental data, taking into account various contributions. The contributions to the exposure dose returned by the fitting routine are plotted *vs.* repetition rate in the small panels below the main plots. The dashed lines in the main panels are guides to the eye corresponding to Eq. (2) for different values of N.

#195297 - $15.00 USD Received 6 Aug 2013; revised 14 Oct 2013; accepted 15 Oct 2013; published 25 Oct 2013

Table 2. Excited-state energies and ionization potentials of the molecules under investigation determined numerically using the OVGF method. The corresponding number of excitation photons (1.55 eV) with the same energy is also given.

Substance	S_0-S_1 energy (eV)	corresponding # of photons	Ionization energy (eV)	corresponding # of photons
PETA	4.8	3.1	10.7	6.9
Irgacure 369	3.9	2.5	7.9	5.1
Irgacure 819	3.3	2.1	8.7	5.6
DETC	3.1	2	7.9	5.1

photoionization of the monomer molecule (compare Table 2). The fit (red line in Fig. 2) nicely reproduces the experimental data. The contributions of the two channels to the total exposure dose are calculated from the fit coefficients a_N as $D_N/D_{\mathrm{acc}} = R \cdot a_N \cdot {E_\mathrm{p}}^N$ and plotted in the small panels below the main graphs. The main contribution stems from a highly non-linear process with $N = 7$, clearly incompatible with the picture of two-photon absorption. Although we do not claim to fully understand or model the photoresist system, this $N = 7$ process appears consistent with a multi-photon photoionization of the monomer molecules creating the initiating species.

3.1.2. Photoresists B and C

For the common sensitized photoresists B and C, we use a fit using the relations $D_{\mathrm{acc}} = a_2 \cdot {E_\mathrm{p}}^2 + a_5 \cdot {E_\mathrm{p}}^5$ (resist B) and $D_{\mathrm{acc}} = a_2 \cdot {E_\mathrm{p}}^2 + a_6 \cdot {E_\mathrm{p}}^6$ (resist C). The contributions correspond to a two-photon excitation and a multi-photon photoionization of the initiator molecules (see Table 2). The absorption found for the pure monomer is probably also present in this case. However, we find that omitting the monomer contribution does not alter the outcome of the fits significantly.

For high repetition rates between 100 kHz and 80 MHz, the $N = 2$ process is clearly dominating, consistent with the classical picture of a two-photon absorption mechanism. For repetition rates below 10 kHz, a process of higher non-linearity becomes dominant. This observation is consistent with a photoionization of the photoinitiator molecules dominating over the two-photon absorption channel.

It should be noted that the high non-linearity at low repetition rates could also have different reasons. For example, this behavior could be caused by the complex polymerization chemistry that we have neglected so far: In the extreme case of low repetition rates and high pulse energies, the dynamics of the polymerization reaction changes considerably. A first laser pulse generates a large amount of primary radicals. These mobile molecules recombine quickly to some extent and only the remaining radicals initiate the polymerization. The radicals generated by a second laser pulse do not only recombine with each other, but also terminate the propagating polymer chains initiated by the first laser pulse. It is often assumed, that chain-chain termination between two pulses is low and that nearly every chain propagates from one laser pulse until the arrival of the next laser pulse. (This assumption is the basis of the pulsed-laser-polymerization technique used to determine propagation constants of monomer molecules [24].) However, the primary radicals remaining after the recombination phase initiate the same number of propagating chains that have been terminated previously. Hence, the number of propagating chains is not influenced by the second laser pulse. Accordingly, for fixed pulse energy and exposure time, the polymer conversion would become independent of the repetition rate. In our evaluation, this extreme case would correspond to $N = \mathrm{inf}$. The increased non-linearity in our experimental data may thus be the very beginning of a transition towards this regime.

#195297 - $15.00 USD Received 6 Aug 2013; revised 14 Oct 2013; accepted 15 Oct 2013; published 25 Oct 2013

On the other hand, for very high pulse energies, the fraction of primary radicals that remains after the initial fast recombination phase becomes independent of the actual pulse energy, because the fast bimolecular recombination continues until the concentration is decreased to a certain value. However, this effect would lead to an effectively decreased non-linearity, just opposite to our experimental observation experimental observation.

Another explanation for the higher non-linearity might be that the photoinitiator molecules are excited to higher singlet states *via* excited-state absorption. These states may possess a higher yield for radical generation or generate radicals that are more reactive towards the monomer.

Concerning heat-accumulation, we do not find a characteristic change that has been reported to be at around 200 kHz [9] or 1 MHz [14] in our data. Moreover, we find no region where the polymerization threshold fits the $N = 1$ dependence that was predicted as a sign for avalanche ionization [9] (see gray dashed line in Fig. 2).

3.1.3. Photoresists D

Photoresist D is based on the DETC photoinitiator which can also be used for stimulated-emission depletion lithography beyond the diffraction limit [10, 25]. Interestingly, we do not find the anticipated $N = 2$ behavior for any repetition rate regime. Instead, the polymerization threshold can in principle fitted with $N = 3$ over nearly the entire repetition-rate range. As two photons should be sufficient to drive the S_0-S_1 transition, this behavior is unexpected and subject to future investigations. A fit using the relation $D_{\mathrm{acc}} = a_3 \cdot {E_{\mathrm{p}}}^3 + a_6 \cdot {E_{\mathrm{p}}}^6$ reveals that in addition to the apparent three-photon absorption a higher-order process contributes significantly at low repetition rates. Again, this process is compatible with a multi-photon photoionization of the photoinitiator molecule. However, no $N = 1$ dependence and no onset of heat accumulation is observed.

3.1.4. Comparison to literature two-photon absorption cross-sections

As the photoresists B and C show the $N = 2$ behavior expected for two-photon absorption (2PA), we want to compare our results to 2PA cross-sections known from the literature [26]. The photoinitiators Irgacure 369 and 819 have peak 2PA cross-sections of $\sigma_{\mathrm{2PA,peak}} = 27\,\mathrm{GM}$ and $\sigma_{\mathrm{2PA,peak}} \leq 5\,\mathrm{GM}$, respectively [26]. Assuming for these molecules that the 2PA spectrum has the same shape as the one-photon absorption (1PA) spectrum [26], we can estimate the 2PA cross-section at 800 nm wavelength to be $\sigma_{\mathrm{2PA,800\,nm}} = \sigma_{\mathrm{2PA,peak}} \cdot \frac{\sigma_{\mathrm{1PA,400\,nm}}}{\sigma_{\mathrm{1PA,peak}}} = 0.27\,\mathrm{GM}$ and $\sigma_{\mathrm{2PA,800\,nm}} \leq 0.375\,\mathrm{GM}$. Besides the similar value of $\sigma_{\mathrm{2PA,800\,nm}}$, also the molar concentrations in photoresists B and C are similar ($6.4 \times 10^{-2}\,\frac{\mathrm{mol}}{\mathrm{L}}$ and $5.6 \times 10^{-2}\,\frac{\mathrm{mol}}{\mathrm{L}}$, corresponding on average to one molecule in every $3\,\mathrm{nm} \times 3\,\mathrm{nm} \times 3\,\mathrm{nm}$ cube). Assuming that for both molecules the radical generation yield and radical reactivity is comparably high, the experimentally determined similar sensitivities of photoresists B and C is reasonable.

For photoresist C, the scaling does not follow the anticipated $N = 2$ behavior. Hence, there is no point in relating the sensitivity to a 2PA coefficient of DETC.

Finally, we briefly estimate the number of absorption events using these coefficients. To estimate the absorption probability, we start with

$$\frac{\mathrm{d}\Phi}{\mathrm{d}z} = -\sigma_{\mathrm{2PA}} \cdot c_N \cdot \Phi^2\,, \tag{4}$$

where Φ is the photon flux and c_{N} is the number of photoinitiator molecules per volume [27]. We derive the probability for a molecule to be excited *via* 2PA during a single laser pulse to be

$$p_{\mathrm{abs}} = 0.5 \cdot \frac{-\sigma_{\mathrm{2PA}} \cdot E_{\mathrm{p}}^2}{\tau \cdot A_{\mathrm{focus}}^2 \cdot (\hbar\omega)^2}\,, \tag{5}$$

#195297 - $15.00 USD Received 6 Aug 2013; revised 14 Oct 2013; accepted 15 Oct 2013; published 25 Oct 2013

where E_p is the excitation pulse energy, τ is the pulse duration, A_focus is the lateral area of the focal intensity distribution, and $\hbar\omega$ is the photon energy. In the following estimation, we assume a circular top-hat beam profile with area $A_\mathrm{focus} = \pi \cdot (165\,\mathrm{nm})^2$, a top-hat temporal pulse shape with duration $\tau = 200\,\mathrm{fs}$, and a writing velocity of $100\,\mu\mathrm{m/s}$ corresponding to 3.3 ms exposure time.

At a repetition rate $R = 80\,\mathrm{MHz}$, every molecule is exposed to 264000 pulses during the exposure time. At the determined threshold pulse-energy of $E_\mathrm{p} = 0.023\,\mathrm{nJ}$, every molecule is excited with a probability of $p_\mathrm{abs} \approx 0.008\%$ per pulse and is hence expected to get excited 21 times during the exposure time (assuming immediate decay to the ground-state). For the rather repetition rate low $R =$ 128kHz, every molecule is exposed to only 422 pulses. Here, with $E_\mathrm{p} = 0.41\,\mathrm{nJ}$, we get $p_\mathrm{abs} \approx 2.52\%$ and 11 excitations per exposure time. Clearly, for these repetition rates the absorption induced by a single pulse is far from saturation. Moreover, even with decent radical-generation quantum-yields on the order of 10% we can assume that a substantial portion ($\approx 70\%$) of the photoinitiator molecules generates a radical during the exposure time. In contrast to previous considerations [8, 9], these numbers affirm that two-photon excitation and chemical bond breaking are sufficient to explain the polymerization initiation at high repetition rates.

3.2. Damage threshold

There exists another threshold energy beyond which no controlled polymerization can be achieved but rather micro-explosions do occur. While the polymerization threshold is well reproducible within few percent of pulse energy, the damage threshold is harder to determine. These micro-explosions might be seeded by microscopic impurities of the photoresist that may efficiently absorb the laser light *via* one-photon absorption. At high repetition rates, such erratically occurring explosions usually grow bigger and bigger very fast as consecutive laser pulses seem to further heat these regions. For low repetition rates, the micro-explosions seeded by few laser pulses tend to recover instead of escalating. The resulting polymer structure is damaged, yet not completely destroyed (it may exhibit holes from the bubbles generated during the micro-explosions as shown in [8]).

The damage-threshold pulse-energies determined during the writing process are plotted as black stars in Fig. 2. For the pure monomer, the explosion threshold at low repetition rates follows an $N = 7$ behavior, just like the polymerization threshold. This indicates that not a single laser pulse leads to the explosion, but that some kind of accumulation is present. Otherwise, the damage-threshold pulse-energy should be independent of the repetition rate. For repetition rates between $R = 128\,\mathrm{kHz}$ and $R = 512\,\mathrm{kHz}$ a transition-like behavior is observed that might be related to the onset of heat accumulation (like previously suggested for the polymerization process [9]). For even higher repetition rates, a behavior similar to that at low repetition rates is observed, yet at a lower pulse-energy level – possibly due to the amplification through heat accumulation.

Interestingly, the explosion thresholds of the sensitized photoresists B–D closely follow that of the monomer, plotted as gray area in all panels of Fig. 2. Hence, the addition of photoinitiator significantly lowers the polymerization threshold, but hardly lowers the damage threshold. The damage threshold appears to be dominated by the monomer properties.

3.3. Dynamic Range

As a consequence of the last observation, sensitized photoresists will in general possess a larger processing window of pulse energies between polymerization and damage. We characterize this window by the "dynamic range" that we calculate as $E_\mathrm{damage}/E_\mathrm{th} - 1$. In Fig. 3, we plot the dynamic range in percent extracted from the above data.

#195297 - $15.00 USD Received 6 Aug 2013; revised 14 Oct 2013; accepted 15 Oct 2013; published 25 Oct 2013

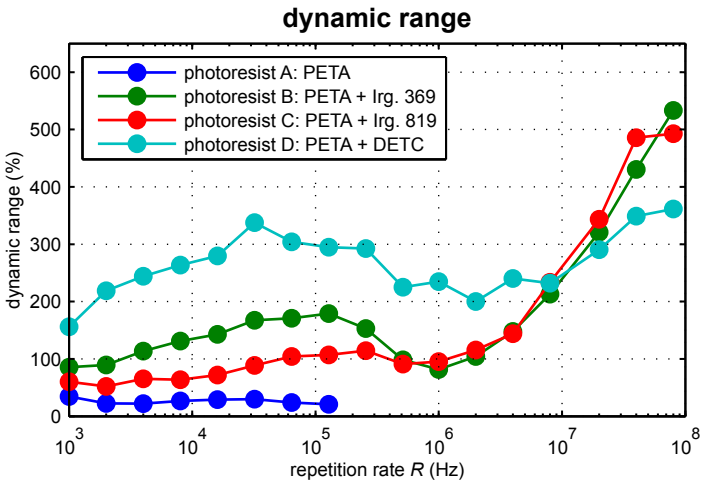

Fig. 3. Dynamic range of the different photoresists as a function of repetition rate R calculated from the data shown in Fig. 2.

As mentioned previously, resist A (the pure monomer) can only be structured with small repetition rates. Hence, the dynamic range is undefined above $R = 128\,\mathrm{kHz}$. The remaining photoresists B–D have a reasonable dynamic range for both high and low repetition rates. For intermediate rates around $R = 1\,\mathrm{MHz}$, the dynamic range is lowered for all photoresists. This is due to the low monomer-explosion threshold in this region, possibly due to the onset of heat accumulation in the damage process. Among the examined resists, the DETC-based photoresist D has the highest dynamic range in this critical repetition-rate range. The practical consequences for DLW in the $R = 1\,\mathrm{MHz}$ regime will be pointed out in Section 5.

4. Polymer linewidths

4.1. Linewidth considerations

As mentioned in Section 1, it seems to be common practice to measure the resulting polymer linewidths in DLW at different writing pulse-energies. We want to show that these investigations do not reveal anything about the nature of the absorption process – at least within the simple model that we use in this paper and that we think is implicitly used by many other authors in the community. For convenience, we consider the exposure dose of a single laser pulse that is absorbed by a non-linear N-photon-absorption process. Moreover, we restrict ourselves to a single lateral spatial direction x. The exposure dose distribution then reads:

$$D(x) \propto \int_{\mathrm{pulse}} \mathrm{d}t I(x,t)^N = (I_0 \cdot f(x))^N \int_{\mathrm{pulse}} \mathrm{d}t\, g(t)^N . \tag{6}$$

Here, $I(x,t) = I_0 \cdot f(x) \cdot g(t)$ is the intensity distribution in the laser focus during the pulse, I_0 is the peak intensity, and $f(x)$ and $g(t)$ are unit-less functions of the spatial and temporal pulse profiles ranging between 0 and 1. The integration over the temporal profile yields a factor that we name c_N and therefore the dose becomes

$$D(x) \propto (I_0 \cdot f(x))^N \cdot c_N \tag{7}$$

For a Gaussian spatial intensity profile $f(x)$ with a spatial FWHM of $\sqrt{2\ln(2)}w_0$, the exposure dose reads

#195297 - $15.00 USD Received 6 Aug 2013; revised 14 Oct 2013; accepted 15 Oct 2013; published 25 Oct 2013

$$D(x) \propto \left(I_0 \, \mathrm{e}^{\frac{-2x^2}{w_0^2}} \right)^N \cdot c_N \,. \tag{8}$$

Now we set this expression equal to the threshold exposure-dose D_{th}. Using the relation in Eq. (7), the threshold dose can be translated to a threshold intensity: $D_{\mathrm{th}} \propto I_{\mathrm{th}}^N \cdot c_N$. This means that I_{th} is the peak intensity that locally leads to the threshold exposure-dose *via* N-photon absorption. From $D_{\mathrm{th}} = D(x)$ we get

$$I_{\mathrm{th}}^N \cdot c_N = \left(I_0 \, \mathrm{e}^{\frac{-2x^2}{w_0^2}} \right)^N \cdot c_N \,. \tag{9}$$

Solving for $2x$ gives the diameter of the region that exceeds the threshold:

$$\mathrm{Linewidth}(I_0) = 2x = w_0 \sqrt{2 \ln \left(\frac{I_0}{I_{\mathrm{th}}} \right)}. \tag{10}$$

If we now experimentally examine the dependence of the linewidth on the pulse energy and leave all other parameters constant (writing velocity, pulse duration, repetition rate, focus diameter), we actually vary I_0. As we can see in Eq. (10), the shape of the corresponding function does depend on the known focal width w_0 and the usually unknown threshold intensity I_{th}. The shape does not depend on N. In particular, the peak intensity I_0 does not enter as I_0^N as one could have expected [28].

The fact that a pure laser-power sweep should not give information about the absorption/initiation process is neither restricted to absorption processes of the form $I(x,t)^N$, nor to Gaussian spatial intensity profiles. We can use a generic absorption process with the absorption rate $h(I)$ that shall be monotonically increasing with I. The general intensity profile is described by $I(x,t) = I_0 \cdot f(x) \cdot g(t)$. The exposure dose and threshold equation now read:

$$D(x) \propto \int_{\mathrm{pulse}} \mathrm{d}t \; h(I(x,t)) = \int_{\mathrm{pulse}} \mathrm{d}t \; h(I_0 \, f(x) \, g(t)) \tag{11}$$

$$\int_{\mathrm{pulse}} \mathrm{d}t \; h(I_{\mathrm{th}} \, g(t)) = \int_{\mathrm{pulse}} \mathrm{d}t \; h(I_0 \, f(x) \, g(t)) \tag{12}$$

For a given $g(t)$ and a monotonically increasing $h(I)$, we can simplify this expression to

$$I_{\mathrm{th}} = I_0 \, f(x) \tag{13}$$

and deduce a linewidth of

$$\mathrm{Linewidth}(I_0) = 2x = 2 \cdot f^{-1}(I_{\mathrm{th}}/I_0), \tag{14}$$

where f^{-1} is the inverse function of $f(x)$. Again, the shape of the diameter function is only influenced by the spatial intensity profile $f(x)$. The nature of the absorption process (included in $h(I)$) does not enter.

4.2. Linewidth measurements

We experimentally examine the width of the resulting polymer lines for the different photoresists and repetition rates. We restrict ourselves to three repetition rates representing the three regimes found in Fig. 3: a low ($R = 4\,\mathrm{kHz}$), a medium ($R = 1\,\mathrm{MHz}$), and a high repetition rate ($R = 80\,\mathrm{MHz}$). We write a test pattern directly at the substrate-photoresist interface and afterwards characterize the developed samples with a scanning electron microscope (SEM). We

#195297 - $15.00 USD Received 6 Aug 2013; revised 14 Oct 2013; accepted 15 Oct 2013; published 25 Oct 2013

believe that using lines attached to the substrate is a more reliable method than using lines inside the resist volume spanned between massive polymer supports [9, 17, 29]. Such lines tend to shrink significantly and their final extend may in some cases be dominated by shrinkage [29]. As the shrinkage depends on the degree of conversion of the polymer lines, which in turn depends on the exposure dose, such measurements of linewidth *vs.* pulse-energy may be corrupted. In contrast, lines rigidly attached to the substrate surface show low shrinkage and allow for less disturbed measurements.

However, an accurate and reproducible finding of the glass-photoresist interface is necessary for this method. Therefore, the sample tilt with respect to the lateral *x*-*y* scanning plane is measured and compensated for. Moreover, every pattern is repeated for different *z*-positions (within $\pm 150\,\mathrm{nm}$ from the nominal position) and the "optimal" *z*-position (that neither exhibits lines fallen over nor lines with a seemingly increased threshold) are used for the evaluation.

Finally, the linewidths are then manually extracted from high-resolution SEM images. The resulting linewidths *vs.* pulse energies are plotted in Fig. 4 as blue dots.

As explained in Section 4, we expect the form of the linewidth-*vs*.-energy curve not to depend on the nature of the non-linear process. Therefore, we fit all experimental data sets according to Eq. (10). For w_0, we use a common value of 314.2 nm for all fits. The corresponding FWHM of the focal intensity distribution (370 nm) is slightly larger than the value we measure (360 nm) when characterizing the focus by a gold-bead scanning method (see, *e.g.*, Ref. [21]). As expected, despite the seemingly different absorption mechanisms ranging between $N = 2$ and $N = 7$, all data are fitted nicely up to linewidths of around 450 nm. Larger linewidths show some deviations from the above simple threshold model. This can be partially explained by the actual focal shape that also differs from an ideal Gaussian for larger distances from the optical axis.

In direct comparison to Ref. [9], we do indeed find a roughly linear scaling for photoresist B at high repetition rates (photoresist B uses the same photoinitiator as Ref. [9]). However, we do not see any difference between very high and very low repetition rates. Therefore, the proposed sign for a transition from heat-accumulation-free to heat-accumulation-dominated polymerization at around 200 kHz can not be found in our resist system and for our femtosecond-pulse system. One should note, however, that we use a liquid monomer instead of the gel-like monomer in [9]. The potentially different thermal conductances of the photoresists and the different pulse durations may cause this discrepancy.

The minimum achievable linewidth seems to be smallest for the unsensitized photoresist A (in agreement to earlier observations [8]). For all other resists and repetition rates, no clear trend is visible. Equation 10 does not predict a minimum linewidth as it assumes a perfectly sharp threshold. A microscopic treatment, using modeling as a percolation problem, reveals that for common experimental parameters feature sizes below 100 nm lead to strongly increased fluctuations of the feature size and the feature position [30], resulting in a blurred effective threshold. Therefore, the linewidth is likely limited by the contrast between the threshold exposure-dose and the peak exposure-dose in the center of the focal spot. When aiming for small features, this contrast is reduced. As a result, the polymerized feature shows low conversion, weak mechanical stability, and low reproducibility. It is important to note that - in sharp contrast to the linewidth scaling - this exposure-dose contrast is indeed influenced by the non-linearity of the photoresist response: The higher the non-linearity, the sharper is the exposure dose profile and the higher is the exposure-dose contrast for a given feature-size. This explains why the unsensitized photoresist enables somewhat smaller feature sizes.

#195297 - $15.00 USD Received 6 Aug 2013; revised 14 Oct 2013; accepted 15 Oct 2013; published 25 Oct 2013

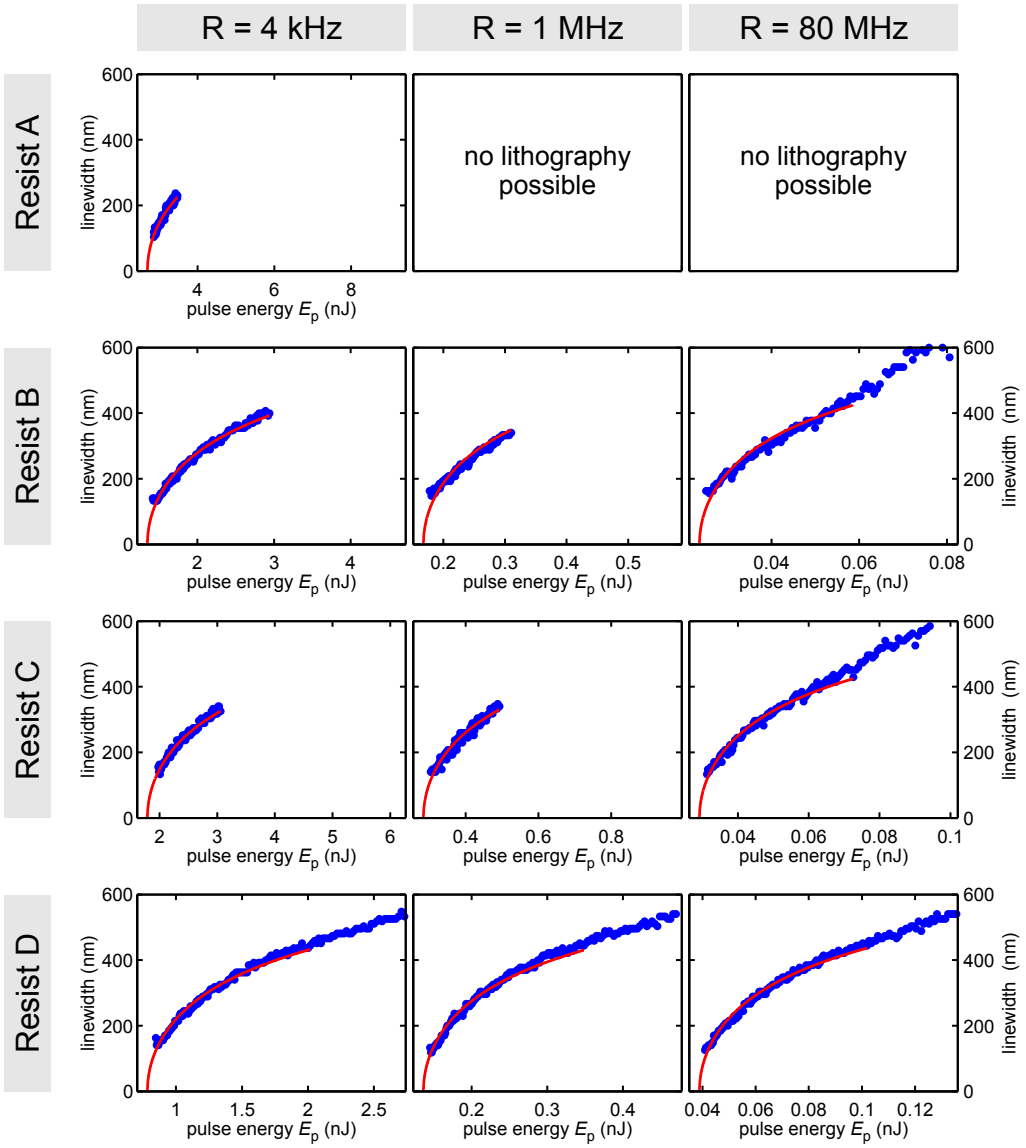

Fig. 4. Experimentally determined linewidths for different photoresists and repetition rates plotted *vs.* the writing pulse energy. Blue dots are actual data points, red lines are fits according to Eq. (10). All fits have a common fit parameter $w_0 = 314.2\,\text{nm}$, corresponding to 370 nm intensity FWHM of the writing spot.

5. 3D Resolution

We have seen in the previous Section that the attainable minimum linewidth and the functional dependence on the pulse energy do not change when changing the repetition rate – despite the different effective non-linearities. In sharp contrast, the resolution – which is defined by the smallest attainable period or distance between multiple exposed features – is expected to change [11]. The higher the non-linearity, the higher the resolution should be.

In order to study the 3D resolution of the different photoresists and different repetition rates,

#195297 - $15.00 USD Received 6 Aug 2013; revised 14 Oct 2013; accepted 15 Oct 2013; published 25 Oct 2013

we fabricate several series of woodpile photonic crystals with different lattice constants and writing pulse-energies (see Fig. 5). The data can be directly compared to earlier studies on diffraction-unlimited DLW [10]. The woodpiles have a footprint of $20\,\mu\text{m} \times 20\,\mu\text{m}$ and lateral rod spacings between $a = 450\,\text{nm}$ and $a = 300\,\text{nm}$. The pulse energy is increased along the horizontal direction of the image in steps of 1%. The writing velocity is chosen as $100\,\mu\text{m/s}$. The axial period – which is actually the limiting one in terms of resolution [10] – is $c = \sqrt{2}\,a\,s$, where $s = 1.28$ is a shrinkage pre-compensation factor. We chose the same three representative repetition rates as in the previous section.

We calculate the critical axial rod separation according to a multi-photon adopted Sparrow criterion using the approximation formula given in [11]:

$$\Delta z_{\text{min}} = \frac{\lambda\,\text{AR}}{2\text{NA}\sqrt{N}} = \frac{3}{4}c\,, \tag{15}$$

where $\lambda = 800\,\text{nm}$ is the exposure wavelength, $\text{AR} = 2.5$ is the aspect ratio (i.e., the ratio between voxel height and width), $\text{NA} = 1.4$ is the numerical aperture of the objective lens, and N is the order of the multi-photon-absorption process.

Along the lines of Ref. [10] and for a woodpile photonic crystal, this corresponds to a minimum lateral rod spacing

$$a_{\text{min}} = \frac{2}{3}\frac{\lambda\,\text{AR}}{s\,\text{NA}\sqrt{2N}}\,. \tag{16}$$

To compare the experimental results to our resolution expectation, we estimate the non-linearity N for all writing conditions using the local slopes of the curves in Fig. 2 together with Eq. (2). The evaluation of Eq. (16) then yields the critical a_{min}-values that we put along-side with the experimentally found a_{exp} in Table 3. Clearly, for larger N-values we expect smaller a_{min}-values and, hence, higher resolution.

Reflection-mode optical micrographs of the final structures are depicted in Fig. 5. We want to emphasize that all structures were fabricated on a single glass substrate with four resist droplets. In this way, all samples share the same setup, laser alignment, power calibration, and development process and a maximum comparability is guaranteed. Moreover, the entire sample was fabricated a second time with very similar outcome so that we can be sure that the below observations are not statistical in nature. The achievable resolutions judged by the occurrence of Bragg-reflection colors are summarized in Table 3. As described in [10], very small structures fabricated at close-to-threshold conditions slightly degrade in quality within the first day after development. The structures shown in this publication were examined directly after development and, hence, the final structure quality will be somewhat lower.

For photoresist A (*i.e.*, pure PETA monomer), only low-repetition rate structuring was successful, while at higher repetition rates pronounced micro-explosions occurred. The smallest structures showing Bragg-reflection colors have $a = 300\,\text{nm}$. This value was so far only achieved using the super-resolution approach presented in [10] but is easily explained by the high non-linearity the photoresist shows in this repetition-rate region ($N = 7$, compare Fig. 2 and Tab. 3).

For photoresist B containing Irgacure 369 as photoinitiator, structuring was successful for $R = 80\,\text{MHz}$ and $R = 4\,\text{kHz}$. At the intermediate repetition rate $R = 1\,\text{MHz}$, structuring was prevented by micro-explosions. Note that according to Fig. 3 the dynamic range for $R = 1\,\text{MHz}$ should be higher than the corresponding dynamic range of the pure monomer at low repetition rates. However, when aiming for a woodpile structure, many densely packed exposures increase the risk for micro-explosions. As mentioned in Section 3, these explosions have a catastrophic impact at high repetition rates, while they are rather forgiving at low repetition rates. This explains why structuring is possible for photoresist A at $R = 4\,\text{kHz}$ – despite the smaller dynamic

#195297 - $15.00 USD Received 6 Aug 2013; revised 14 Oct 2013; accepted 15 Oct 2013; published 25 Oct 2013

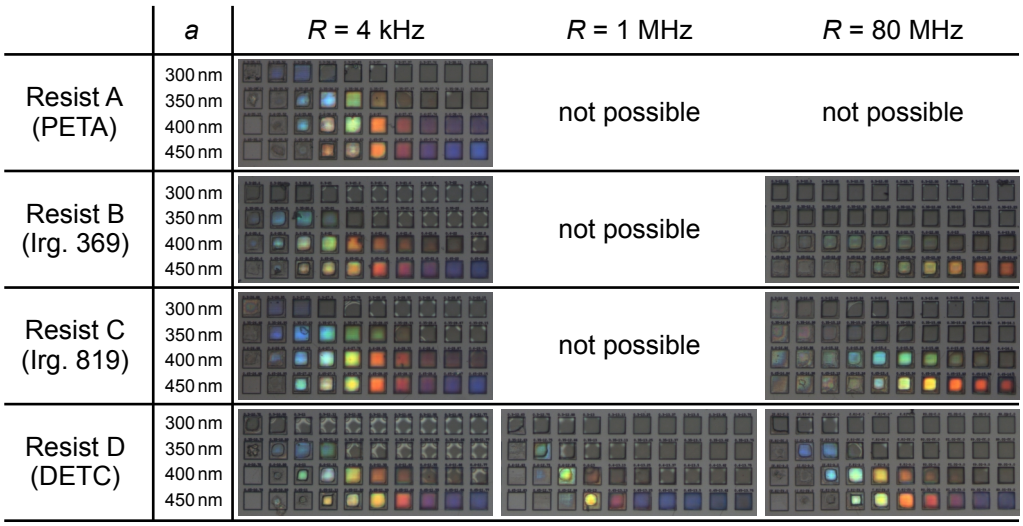

Fig. 5. Optical micrographs (reflection mode) of woodpile photonic crystals with different lateral rod spacings a. The axial layer separation is scaled accordingly. The results for different photoresists and repetition rates can be compared. Missing fields are due to micro-explosions having prevented successful fabrication. The rod distance a is decreased along the vertical direction as indicated. In the horizontal direction, the exposure pulse energy is increased from left to right in relative steps of 1%.

Table 3. Summary of the 3D resolution tests: Achievable minimum lateral rod spacing a_{exp} of woodpile photonic crystals. The non-linearity N together with the anticipated minimum rod spacing a_{min} according to the multi-photon Sparrow criterion (Eq. (16)).

		Resist A	Resist B	Resist C	Resist D
$R = 4\,\mathrm{kHz}$	N	7	3.5	4.5	4
	a_{min}	199 nm	281 nm	248 nm	263 nm
	a_{exp}	300 nm	350 nm	300 nm	350 nm
$R = 1\,\mathrm{MHz}$	N	–	2	2	3
	a_{min}	–	372 nm	372 nm	304 nm
	a_{exp}	–	–	–	350 nm
$R = 80\,\mathrm{MHz}$	N	–	2	2	3
	a_{min}	–	372 nm	372 nm	304 nm
	a_{exp}	–	400 nm	400 nm	350 nm

range. As predicted by the threshold data, the resolution at repetition rate $R = 4\,\mathrm{kHz}$ is significantly higher than for $R = 80\,\mathrm{MHz}$. The achievable rod distances (see Table 3) are in reasonable agreement with the values predicted by the multi-photon Sparrow criterion.

For photoresist C containing Irgacure 819 as photoinitiator, the overall behavior is very similar to photoresist B. The overall quality seems somewhat better than for photoresist B. For the low repetition rate $R = 4\,\mathrm{kHz}$, higher resolution is observed compared to photoresist B. This is consistent with the stronger non-linearity and matches the predicted values (Fig. 3).

For photoresist D containing DETC as photoinitiator, structuring is also possible for the intermediate repetition rate $R = 1\,\mathrm{MHz}$, although the fabrication window is also very narrow. For the high and low repetition rate, the quality is roughly equal, which is consistent with the nearly constant non-linearity for all repetition rates (see constant slope for photoresist D

#195297 - $15.00 USD Received 6 Aug 2013; revised 14 Oct 2013; accepted 15 Oct 2013; published 25 Oct 2013

in Fig. 2). At high repetition rates, DETC offers higher resolution than the other photoresists under investigation, consistent with the higher non-linearity ($N = 3$ compared to $N = 2$).

6. Conclusion

We have conducted systematic DLW experiments with different repetition rates. We find that for common sensitized photoresists based on Irgacure photoinitiators, the polymerization is clearly induced by two-photon absorption at high repetition rates. The observed threshold-scaling is perfectly described by this mechanism for all repetition rates above 100 kHz. An estimate of the two-photon absorption rates based on literature cross-section values further affirms this finding. For low repetition rates, the process appears to be more non-linear. This observation is consistent with a photoionization mechanism at low repetition rates. For the polymerization, we find that heat accumulation is not evident from our data. For the damage mechanism, however, a transition consistent with heat accumulation is found. In this region around 1 MHz repetition rate, micro-explosions are most pronounced and the fabrication window is smallest. Hence, this repetition-rate range should be avoided.

We expect and experimentally verify that the dependence of the resulting polymer linewidth on the writing pulse-energy is independent of the non-linearity of the absorption/initiation process. We find no influence of the repetition rate on the linewidth scale, despite the large repetition-rate interval we have examined. Hence, the significance of corresponding examinations in previous publications appears questionable.

Moreover, we find that high-resolution patterning is possible with the unsensitized monomer as photoresist for low repetition rates only. For common sensitized photoresists (photoresists B and C), low repetition rates yield higher resolution than high repetition rates. At high repetition rates, the photoresist sensitized with the uncommon photoinitiator DETC offers the best resolution in the test field. The resolutions for all conditions are reasonably predicted by the multi-photon Sparrow criterion introduced previously [11]. The largest deviation is found for the pure monomer which should offer even higher resolution according to the formula. This may be an indication that the resolution of this photoresist is actually limited by effects like diffusion and not by optics. We find that increasing the photoresist sensitivity does not increase the resolution (contradicting Ref. [6]) but only increases the dynamic range. For low repetition rates, the sensitization even decreases the resolution, as it decreases the non-linearity of the process towards $N = 2$.

Finally, the data of this paper covering repetition rates over nearly five orders of magnitude should provide valuable guidance to experimentalists and engineers regarding the design and scaling of future DLW systems at uncommon repetition rates.

Acknowledgments

We acknowledge support by the Deutsche Forschungsgemeinschaft (DFG), the State of Baden-Württemberg, and the Karlsruhe Institute of Technology (KIT) through the DFG Center for Functional Nanostructures (CFN) within subprojects A1.04, A1.05, and C3.02U and through Open Access Publishing Fund of KIT. The PhD education of J. K. and J. M. is embedded in the Karlsruhe School of Optics & Photonics (KSOP).

#195297 - $15.00 USD Received 6 Aug 2013; revised 14 Oct 2013; accepted 15 Oct 2013; published 25 Oct 2013